Environmental Science Nano

ROYAL SOCIETY OF CHEMISTRY

PAPER

View Article Online
View Journal | View Issue

Cite this: *Environ. Sci.: Nano*, 2024, **11**, 1114

Multifunctional halloysite nanotube–polydopamine agro-carriers for controlling bacterial soft rot disease†

Sandeep Sharma, ‡ Ofer Prinz Setter,‡ Hanan Abu Hamad and Ester Segal *

Current pesticide formulations suffer from instability and susceptibility to drift, which diminish their effectiveness and harm the environment. To circumvent these challenges, we have developed a core–shell carrier by employing *in situ* polymerization of dopamine on halloysite nanotubes (HNTs), loaded with the antibacterial essential oil thymol. This hybrid system demonstrates a 2.5-fold higher content of loaded thymol and a 3-fold slower release rate compared to a control lacking the 10 nm thick polydopamine layer. Additionally, the polydopamine coating confers dual-stimuli responsiveness to both acidic pH (mimicking plant infection sites) and near-infrared (NIR) irradiation (mimicking natural sunlight). Consequently, the functionalized clay shows a 2.5-fold increase in inhibiting the major plant pathogen, *Erwinia carotovora*, at pH 5 compared to a neutral pH. A similar trend is observed under NIR irradiation, attributed to the photothermal properties of polydopamine in combination with thymol release. In terms of crop safety, our polydopamine-coated HNT-based nanocarriers are found to be non-phytotoxic to tomato plants and show no evidence of foliar uptake as confirmed by confocal microscopy. The mussel-inspired polydopamine shell also enhances thymol stability under UV irradiation, and improves the wettability and leaf adhesion of the formulation, thereby reducing drift under simulated rainy conditions. Ultimately, the designed hybrid material exhibits superior *in planta* efficacy in controlling soft rot disease in tomato crops. We believe our clay-based core–shell agro-nanocarrier loaded with thymol offers a sustainable alternative to existing pesticide formulations while providing enhanced efficacy, stability, and crop safety.

Received 12th December 2023,
Accepted 30th December 2023

DOI: 10.1039/d3en00934c

rsc.li/es-nano

Environmental significance

Escalating global food demand necessitates extensive use of pesticides, which may contaminate soil and crops, exposing the consumer to toxic biocides. Our sustainable nanoformulation, shown to be highly effective in controlling soft rot disease *in planta*, is composed of natural and biodegradable components: a natural clay carrier, an antibacterial essential oil, that is generally recognized as safe, and the biocompatible polymer polydopamine. Not only does the latter enable the sustained and triggered release of the active compound, but it also enhances foliar adhesion and UV stability of the formulation, minimizing drift and obviating the need for repetitive applications, thus reducing the ecological footprint. Furthermore, we observed no foliar uptake of the applied nanocarrier at the cellular level, mitigating its potential entry into the food chain.

Faculty of Biotechnology and Food Engineering, Technion – Israel Institute of Technology, Haifa – 3200003, Israel. E-mail: esegal@technion.ac.il

† Electronic supplementary information (ESI) available: Additional material in ESI includes the following: standard curve for TY absorbance in ethanol, FTIR spectra of TY and TY-loaded HNTs, TGA and DTG curves of HNTs-based hybrids, TY loading capacity of TY-loaded HNTs and TY-loaded HNTs/PDA hybrid, images showing the effect of TY emulsion, and plain buffer solutions at pH 7 and pH 5 on *E. carotovora* growth, temp. profile of deionized water, HNTs, PDA-coated HNTs, and TY-loaded HNTs/PDA hybrid after irradiation with 808 nm NIR laser, antibacterial activity HNTs and PDA-coated HNTs lacking TY with and without NIR irradiation, fluorescence spectra of FITC-conjugated HNTs and FITC-conjugated PDA-coated HNTs, confocal images of leaves (mesophyll cells and leaf epidermis) after 24 h incubation with FITC-conjugated HNTs and FITC-conjugated PDA-coated HNTs, confocal images of HNTs and PDA-coated HNTs treated leaves after PI-staining, and photographs of uninfected and bacterial infected leaflets treated with deionized water. (PDF). See DOI: https://doi.org/10.1039/d3en00934c

‡ Authors contributed equally to this work.

Introduction

Zero hunger is set as the second sustainable development goal (SDG) of the United Nations towards 2030.[1] One of the main crops that holds ~20% of the global vegetable consumption per year, is tomato (*Solanum Lycopersicum L.*),[2] which is a rich source of vitamins, macro-, and micronutrients, as well as phytochemicals.[3] Yet, tomato production is greatly damaged by the soft rot disease caused by *Erwinia carotovora* (*E. carotovora*),[4,5] manifesting as necrotic spots that rapidly expand on infected areas.[6] Consequently, pesticides including copper cations are extensively used to mitigate this disease.[7,8] However, a significant amount of the applied pesticide formulations is

lost due to drift,[9] which results in repeated pesticide application. Not only is this uneconomical, but it also has severe health and environmental implications,[10–12] and may further induce pathogen resistance.[13–15] This calls for the development of new sustainable formulations that include eco-friendly active ingredients and a carrier for sustained release.

Essential oils (EOs) have emerged as promising candidates for serving as sustainable pesticides that had already evolved through natural selection to protect plants against insects, and pathogenic fungi or bacteria.[16–18] Among EOs, thymol (TY) has attracted significant attention due to its broad-spectrum antimicrobial and insecticidal properties.[19–21] Moreover, several TY-containing formulations are registered as pesticides in beehives by the U.S. Environmental Protection Agency (EPA),[22] and TY is categorized as GRAS (generally recognized as safe) by the U.S. Food and Drug Administration.[23] Nonetheless, the efficacy of TY as a pesticide is limited since it is highly volatile, light sensitive, and poorly soluble in water, resulting in low residual activity.[20,24] To overcome these limitations, TY has been incorporated into various micro- and nano-delivery systems such as starch microspheres, liposomes, and β-cyclodextrin complexes.[20,24–26]

In contrast to such synthetic approaches, natural nanoclays, which are abundant and intrinsically mesoporous, constitute a sustainable and cost-effective alternative.[27,28] One prominent candidate clay is halloysite nanotubes (HNTs), which have been successfully utilized as carriers for TY and other EOs allowing their sustained release.[29,30] HNTs are 1 : 1 aluminosilicate clay minerals and exhibit a unique tubular morphology with characteristic dimensions of 600–900 nm, 50 nm, and 15 nm in length, outer and inner diameter, respectively.[31,32] Recent studies have revealed that HNTs are not more toxic than other high-aspect ratio nanomaterials.[33,34] In addition, HNTs (<1 mg mL^{-1}) were found to be nonphytotoxic to wheat seedlings and even beneficial for the proliferation of tobacco cells.[35] Owing to the abundance of HNTs combined with their beneficial attributes, they have been extensively studied as nanocarriers for numerous bioactive compounds.[36] In addition, HNTs can be physically and chemically modified to endow them with new functionalities and tune the loading and release behavior of guest molecules.[33,37–39]

Polydopamine (PDA), a mussel-inspired biocompatible polymer,[40,41] has been widely investigated in combination with HNTs.[42–44] The catechol side group of PDA chain strongly adheres to both organic and inorganic surfaces through chemical and physical interactions;[45] thus, PDA-coated particles strongly attach to plant leaves, minimizing drift loss,[46] even under humid conditions.[47] In addition, the melanin-like domains in PDA absorb near-infrared (NIR) irradiation,[48] and exhibit photothermal activity that could trigger a pesticidal effect,[43] or the release of active compounds.[49] At the same time, a PDA coating can also shield the active ingredient against UV radiation.[50] Moreover, the polymer degradation under acidic pH,[48,51] facilitates triggered release at low pH values,[52] characteristic of pathogenic infection of plants.[53–57]

In this study, we combine for the first time the three components HNTs, TY, and PDA into an all-natural nano-formulation for plant disease control using tomato as a model plant and *E. carotovora* as a relevant model pathogen responsible for the soft rot disease. HNTs were first loaded with TY and then coated with PDA through the self-polymerization of dopamine in TY-loaded HNTs dispersion. The investigated multifunctional hybrids are shown to promote the following: (1) sustained and pH-triggered release of TY, (2) photo-triggered antibacterial effect, (3) prevention of TY loss under UV radiation, and (4) prolonged pesticidal activity by superior foliar adhesion tested *in planta*.

Experimental

Materials

Halloysite nanotubes were purchased from NaturalNano (USA). Thymol (≥98.5%), tween 80, dopamine hydrochloride (98%), Tris-HCl (>99%), disodium hydrogen phosphate (ACS reagent, ≥99.0%), sodium citrate, (3-aminopropyl) triethoxysilane (APTES), fluorescein isothiocyanate (FITC), propidium iodide (PI), and agar were obtained from Sigma-Aldrich, Israel. Acetone, absolute ethanol, citric acid, and sodium chloride were obtained from BioLab, Israel. Tryptone and yeast extract for Luria-Bertani (LB) medium were supplied by Becton Dickinson (USA). Magnesium chloride (anhydrous, 99%) was purchased from Alfa Aesar, Israel. Sodium dihydrogen phosphate (Reag. Ph Eur) was purchased from Merck, Israel. Citric acid and sodium citrate were used for the pH 5 buffer preparation, and disodium hydrogen phosphate and sodium dihydrogen phosphate were used for the pH 7 buffer preparation. Milli-Q water (18 MΩ cm) was used to prepare all the solutions and is referred to as double-distilled water (DDW) in this work.

Bacterial culture: *E. carotovora Subsp. brasiliensis* was isolated from potatoes and kindly supplied by the Maon Region Communities Cooperative, Israel.

Synthesis of TY-loaded HNTs/PDA hybrids

Thymol loading. HNTs were dried overnight at 150 °C, prior to their use. TY was loaded into HNTs using the solvent evaporation method under vacuum with slight modifications.[38] First, 100 mg of HNTs were dispersed in a solution of 200 mg TY in 5 mL acetone using a sonication bath. The resulting dispersion was subjected to 30 min-long vacuum cycles (10 bar), to facilitate the HNTs lumen air replacement with the acetone-dissolved TY. Then, the pressure was retained at atmospheric pressure and the sample was re-dispersed in acetone (5 mL) by sonication for 30 s and subjected to 30 min-long vacuum cycle. In total, this process was repeated for 5 cycles and the resulting loaded HNTs sample was used for the subsequent dopamine polymerization. Note that TY-loaded HNTs (no PDA), which

were used as a control, were centrifuged and washed with DDW (×3 times) following the loading process.

***In situ* dopamine polymerization.** The resulting TY-loaded HNTs were dispersed in 20 mL of Tris-HCl buffer (10 mM, pH 8.5) and mixed with 1 mL solution of dopamine–HCl (80 mg mL^{-1}) in Tris-HCl buffer for 6 h at room temperature.[58,59] Subsequently, the reaction mixture was centrifuged at 17 000 × *g* for 10 min and the supernatant was discarded. The obtained pellet was washed 3 times with distilled water by centrifugation and dried overnight under vacuum at room temperature. The same procedure was also followed for *in situ* polymerization of dopamine onto pristine HNTs.

Characterization

The morphology of pristine HNTs and HNTs/PDA hybrids was characterized using an FEI Tecnai G2 T20 S-Twin transmission electron microscope (TEM) at an accelerating voltage of 200 keV. The samples were prepared by mounting 5 μL the respective HNTs dispersion (1 mg mL^{-1}) on a carbon type-B grid and dried overnight in a desiccator. Scanning electron microscopy-energy dispersive X-ray (STEM-EDX) measurement was performed by an EDAX EDS detector on samples mounted on nickel grids with a silicon oxide support. EDX data were processed by TIA (TEM Imaging & Analysis) software version 4.12, FEI Company, OR, USA.

Thermogravimetric analysis (TGA) was carried out using a TGA Q5000 instrument (TA Instruments, USA) in a dynamic high-resolution mode (resolution number: 6; sensitivity value: 1). the samples were heated at a rate of 10 °C min^{-1} up to 600 °C. TGA results were analyzed by Universal Analysis 200 version 4.5A build 4.5.0.5 software.

The chemical composition of HNTs before and after modification was investigated by attenuated total reflectance Fourier-transform infrared (ATR-FTIR) spectroscopy using a Thermo 6700 FTIR spectrometer (USA) equipped with a Smart iTR diamond ATR device.

The zeta potential values of pristine and modified HNTs dispersions were measured in aqueous conditions at neutral pH (0.5 mg mL^{-1} in DDW) by a Malvern Zetasizer Nano ZSP instrument (UK) at 25 °C.

The optical absorbance of pristine and modified HNTs dispersions (following each stage of modification) were recorded at a concentration of 1 mg mL^{-1} using a multimode plate reader (Varioskan, Thermo Fisher Scientific, USA).

Quantification of thymol loading

TY content in TY-loaded HNTs and TY-loaded HNTs/PDA hybrids was quantified by its extraction in absolute ethanol. Briefly, TY-loaded samples were dispersed in 1 mL absolute ethanol (5 mg mL^{-1}) and sonicated for 1 h on ice. Afterwards, the samples were centrifuged at 10 000 × *g* for 10 min and the supernatant was collected. Extraction and centrifugation were repeated for two successive cycles, and the collected supernatants were measured for their absorbance at 278 nm using a multimode plate reader. The concentration of TY in respective samples was determined using a calibration curve generated from different TY concentrations (see ESI,† Fig. S1). The TY loading capacity (LC) and encapsulation efficiency (EE) were determined by using the following equations:

$$\text{LC (w/w\%)} = \left(\frac{\text{weight of loaded TY}}{\text{total weight of hybrid}}\right) \times 100\% \quad (1)$$

$$\text{EE (w/w\%)} = \left(\frac{\text{weight of loaded TY}}{\text{weight of TY in loading solution}}\right) \times 100\% \quad (2)$$

Stimuli-responsive thymol release

The release behavior of TY from the different carriers was investigated in different pH buffers at 30 °C under shaking (200 rpm).[60,61] In brief, TY-loaded HNTs/PDA hybrids (1 mg) and TY-loaded HNTs (1.85 mg) were dispersed separately in 1 mL of pH 5 and pH 7 buffers. Note that due to the significant difference in the TY content in these systems, we used different amounts of loaded HNTs and kept the TY content constant at 0.14 mg. At different time intervals, the whole release medium was collected by centrifugation and replaced with an equal volume of fresh buffers. The amount of TY released in different pH buffers was quantified by measuring the TY absorbance at 278 nm.[62] The release experiments were performed in triplicates and the data were plotted as % cumulative release *vs.* time. A double exponential saturation model was fitted for TY release profiles by Prism software (version 9.5.0 (730), GraphPad Software LLC) according to the following equation:

$$R(t) = R_{\text{inf}} + (R_0 - R_{\text{inf}})a_{\text{fast}}e^{-k_{\text{fast}}\cdot t} + (R_0 - R_{\text{inf}})(1 - a_{\text{fast}})e^{-k_{\text{slow}}\cdot t} \quad (3)$$

where, t is the time (h), $R(t)$ is the cumulative release of TY at time t (% accumulative release), R_0 is the cumulative release of TY at the beginning of the experiment, R_{inf} stands for the value of TY cumulative release at infinite time (% accumulative release), a_{fast} is the fraction of release accounted for by the fast component, while k_{fast} and k_{slow} are the rate constants (h^{-1}) for the fast and slow components, respectively, and are constrained as >0. After constraining R_0 to 0, the equation is simplified to:

$$R(t) = R_{\text{inf}}[1 - a_{\text{fast}}e^{-k_{\text{fast}}\cdot t} - (1 - a_{\text{fast}})e^{-k_{\text{slow}}\cdot t}] \quad (4)$$

Antibacterial assay

The antibacterial properties of TY-loaded HNTs/PDA hybrid against *E. carotovora* were characterized *in vitro* by the standard plate count method.[59] To study the effect of pH on bacterial growth, the TY-loaded HNTs/PDA hybrid (0.67 mg) was dispersed in 0.4 mL buffer (pH 5 or pH 7) and mixed with 0.1 mL of bacterial suspension (10^8 CFU mL^{-1}). The effect of NIR irradiation was studied by irradiating (at 808 nm wavelength and a power density of 1.5 W cm^{-2} for 15 min) the latter dispersions using a laser (WSLS-808-007-

H, Wavespectrum Laser Group, Beijing, China) equipped with a fiber collimator (Thorlabs, Newton, NJ, USA). Following the different treatments, the bacterial dispersions were subjected to shaking at 200 rpm for 1 h at 28 °C, decimally diluted, and uniformly spread onto LB agar plates. The plates were then incubated at 28 °C for 16–18 h, and the bacterial colonies were counted using a CLC-330 colony counter (MRC Lab, Israel). Control experiments followed the same protocols for TY-loaded HNTs, TY emulsion (prepared by dispersing a 1 : 1 ratio of TY and Tween 80 in water at a concentration of 2 mg mL^{-1} using probe sonication at 40% amplitude), pristine HNTs, and PDA-coated HNTs. Note that the concentration of TY in TY-loaded HNTs (1.1 mg) and TY emulsion was 80 μg/0.5 mL (equivalent to the conc. of TY in 0.67 mg of TY-loaded HNTs/PDA hybrid) and the concentration of HNTs in pristine HNT and PDA-coated HNTs was 0.6 mg/0.5 mL (equivalent to the conc. of HNTs in 0.67 mg of TY-loaded HNTs/PDA hybrid).

Imaging of fluorescently-labelled HNTs in plants

Preparation of FITC-conjugated HNTs and PDA-coated HNTs. Pristine HNTs were conjugated with FITC after their surface modification with APTES as reported before.[63] In brief, HNTs (150 mg) were dispersed in a solution of APTES (0.3 M) in toluene by sonication (30 min) and refluxed for 20 h at 120 °C under constant stirring. Subsequently, the dispersion was washed several times with toluene to remove the excess organosilane and dried overnight at 120 °C; followed by washing in DDW and drying overnight. The resulting amino-functionalized HNTs (3 mg) were dispersed in 2 mL of 0.1 M carbonate buffer (pH 8) followed by the addition of 0.1 mL FITC solution (13 mM, prepared in DMSO). The resulting mixture was reacted in the dark for 2 days at room temperature under constant stirring. The obtained products were washed several times with DDW to remove the free fluorophore. The latter conjugation step was used to label the PDA-coated HNTs, which already bear free amines on their surface.

Confocal microscopy imaging. The leaves of tomato leaves were treated with HNTs and PDA-coated HNTs (2.5 mg mL^{-1}) and incubated for 24 h (leaves treated with DDW served as a control). 6 mm disks were cut from the treated leaves with the help of a cork borer and mounted in a gel chamber created on a microscope slide. The chamber was filled with glycerol as a mounting medium and sealed with a glass coverslip. The samples were imaged using a ×20 objective lens by using a multiphoton multispectral laser-scanning microscope (Zeiss LSM 510 META NLO). The samples were excited using a 488 nm laser for FITC excitation and a 633 nm laser for chloroplast excitation. The emission of FITC and chloroplast autofluorescence was captured in the range of 500–600 nm and 650–750 nm, respectively. The colocalization of HNTs with the leaf epidermis and mesophyll cells was performed using the Image-J software. The correlation between the chloroplast autofluorescence and FITC fluorescence was analyzed by Pearson's coefficient analysis.

Phytotoxicity study

The phytotoxicity of HNTs and PDA-coated HNTs in tomato leaves was studied by assessing the integrity of the leaf cells membrane, by propidium iodide (PI) staining and subsequent confocal microscopy imaging. The leaves of live plants were treated (by spraying) with HNTs and PDA-coated HNTs dispersions at a concentration of 2.5 mg mL^{-1}. After 1 and 5 days of treatment, leaf discs were collected with a cork borer and incubated in PI solution (10 μg mL^{-1}) for 15 min, after which the samples were thoroughly washed with DDW to remove excess unbound dye. The stained disks were mounted in a gel chamber created on a microscope slide, filled with glycerol as a mounting medium, and sealed with a glass coverslip. The samples were imaged using a 20× objective lens by using a multiphoton multispectral laser-scanning microscope (Zeiss LSM 510 META NLO) at an excitation wavelength of 488 nm and emission was collected between 500–600 nm. The confocal images were used to calculate the percentage of intact cells (depicting no PI-stained nuclei) with respect to the total number of cells.

The effect of the nanotubes on the chlorophyll content was studied for up to 10 days by using a chlorophyll meter (Spad 502 chlorophyll meter).

Wetting and adhesion studies

The wetting behavior of the different aqueous dispersions of HNTs, TY-emulsion, TY-loaded HNTs, and TY-loaded HNTs/PDA hybrid was studied on the tomato leaf surface using a contact angle optical tensiometer (Attension Theta Flow, Biolin Scientific). For measurement, the selected leaves were carefully fixed onto a glass slide using an adhesive double-sided tape.[64] The contact angle (CA) was recorded through the sessile drop method by placing a droplet of 7 μL of the studied dispersion on the adaxial side of the leaf surface. To observe the change in the CA with time, the shape of the droplet was recorded by a camera for up to 10 min with an interval of 60 s and analyzed using the Attension software. The measurements for every sample were recorded in triplicates.

The retention of the different formulations onto the leaf surface was investigated following a previously published procedure;[65,66] where tomato leaves were sprayed with 5 mL of the respective formulations (*i.e.*, pristine HNTs, TY emulsion, TY-loaded HNTs, and TY-loaded HNTs/PDA hybrid) and allowed to dry. The surface of the treated leaves was observed using an upright light microscope (ZEISS Axio Scope A1, Germany) equipped with an Axiocom MRc (ZEISS, Germany) camera. The treated leaves were washed by spraying 5 mL of DDW for 30 s at an angle of 60° and imaged. The data was processed using ZEN blue (Carl Zeiss

Microscopy) software and Z-stack projections images are presented.

In planta antibacterial studies

Plant materials. One month-old tomato plants (Antonella F1, Hazera Seeds Ltd., Israel) were obtained from Hishtil Nurseries (Israel) and grown in 0.5 L pots containing potting mix. The plants were placed in a greenhouse at 28–32 °C and 12/12 h light/dark photoperiod.

***In planta* antibacterial assay.** This study aims to investigate the potential of the different HNTs dispersions to suppress tomato soft rot disease.[67] Tomato plants were randomly selected and divided into 4 groups (5 plants in each group) which were sprayed with the different aqueous formulations (20 mL) *viz.*, pristine HNTs, TY emulsion (0.4 mg mL^{-1}, equivalent to the loaded TY in HNTs), TY-loaded HNTs, and TY-loaded HNTs/PDA hybrid. Note that the concentration of pristine HNTs used was kept constant in these studies (2.6 mg mL^{-1}). After 2 h, the plants were inoculated with *E. carotovora* suspension (with an optical density at 600 nm of 0.1 in 10 mm $MgCl_2$) and covered with transparent plastic bags. After 48 h, the bags were removed, and the plants were maintained at the above-mentioned greenhouse conditions. After 14 days, the disease severity was recorded on a scale of 0–3 as follows: 0 = no symptoms, 1 = few (<10) necrotic spots on a few leaflets, 2 = few necrotic spots on many leaflets, 3 = spots with coalescence on leaflets.[68] The disease severity index (DSI),[69] was calculated by the following equation:

$$\text{DSI}\ (\%) = \frac{\sum(\text{class frequency} \times \text{score of rating class})}{(\text{Total number of observations}) \times (\text{maximal disease index})} \times 100\% \quad (5)$$

where, the class frequency is the number of plantlets kept in each score on scale, the score of rating class refers to the score on scale (either 0, 1, 2, or 3), the total number of observations is the number of plantlets used for the observation, and the Maximal disease index refers to the highest numerical point on a rating scale.

Thymol content following UV irradiation

The capability of TY-loaded HNTs and TY-loaded HNTs/PDA hybrid to retain the TY content was studied with and without irradiation with UV light.[70] The respective samples were dispersed in DDW at a TY concentration of 0.5 mg mL^{-1}. Subsequently, the samples were placed 10 cm under a UV lamp (Hamamatsu, Lightningcure LC8, Japan) at a wavelength of 365 nm and irradiated at 20% intensity of 138 mW cm^{-2} for different periods (12, 24, 48, 96, and 144 h). After irradiation, the residual TY content was extracted from the respective sample using ethanol and quantified by absorbance measurements at 278 nm (Varioskan, Thermo Fisher Scientific, USA). The control dispersions (non-irradiated) were investigated using the same protocol.

Statistical analysis

Origin software (Origin Pro 8.5 Corporation, U.S.) was used to plot the data. Student *t*-test (two-tailed) using GraphPad Prism 8.0 software was performed at a confidence level of 99% to calculate the significance of the difference between groups. The experiments were performed in triplicates and plotted as mean ± standard error. Plots showing no asterisks or "ns" indicate the absence of a significant difference.

Results

Synthesis and characterization of thymol-loaded HNTs/PDA hybrids

The synthesis of TY-loaded HNTs and TY-loaded HNTs/PDA hybrids is schematically illustrated in Fig. 1A. HNTs were loaded with TY using the solvent evaporation method under vacuum,[38] and subsequently subjected to an *in situ* dopamine polymerization. Dopamine self-polymerizes through a series of oxidation, cyclization, and isomerization reactions in mild-basic conditions to form PDA,[71] while the reactions are accompanied by a distinct color change of the TY-loaded HNTs dispersion from whitish to deep brown (Fig. 1A).[48,72]

The morphology and structure of the resulting particles were characterized by TEM and the respective micrographs are presented in Fig. 1B. Indeed, the modified nanotubes show a thin polymer shell that coats their external surface (Fig. 1B-vi), which cannot be observed for the pristine HNTs (Fig. 1B-iii). The pristine HNTs exhibit cylindrical shape with an irregular inner and outer diameter of 10–30 nm and 40–100 nm, respectively (Fig. 1B-i). The HNT lumen is clearly observable as a brighter strip running along the nanotubes longitudinally, revealing open-ended features (Fig. 1B-ii).[73,74] Following polymerization the contrast between the HNT lumen and its external surface is more pronounced in comparison to the neat HNTs, see Fig. 1B-v in comparison to Fig. 1B-iii, as was previously observed.[74] Importantly, higher magnification images, see Fig. 1B-vi and S2 in the ESI,† reveal a thin ~10 nm layer that coats the nanotubes, ascribed to the PDA, and confirms the formation of core–shell nanostructures. STEM-EDX analysis, presented in Fig. 1C-i and S3,† indicates the colocalization of the aluminum compound of the coated-HNTs and a carbonaceous layer. The latter is observed to further extend a few nanometers beyond the outer surface of the HNTs wall and also into the middle section of the profile (position 180–260 nm), characterized by a lower aluminum composition and thus identified as the tube lumen. No elevated carbon content was observed in the profile of the control pristine HNTs (Fig. 1C-ii). Thus, we suggest that the mechanism of the shell formation first involves the adherence of dopamine catechol anchors onto the HNTs surface, *via* various interactions *viz.*, H-bonding

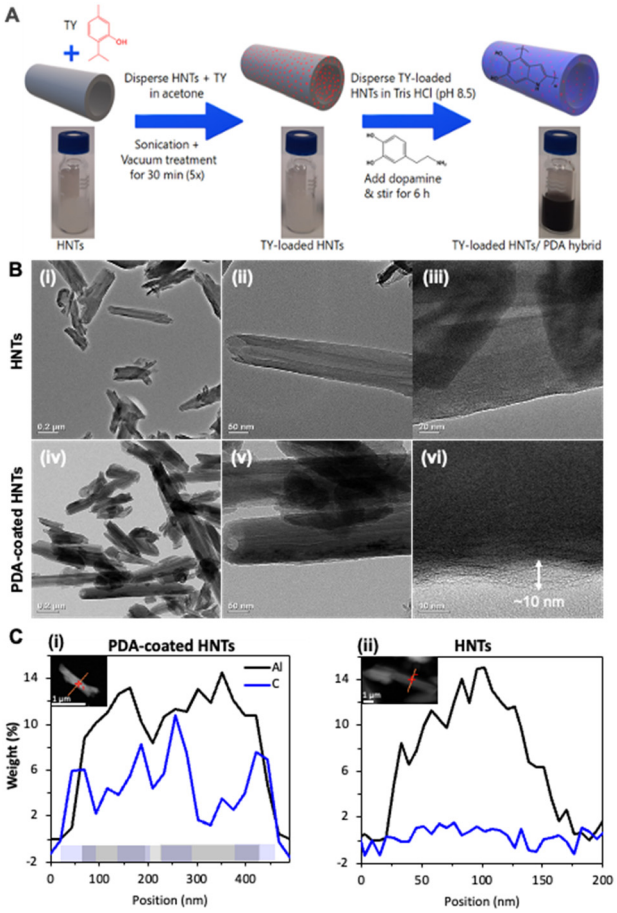

Fig. 1 (A) A schematic illustration summarizing the steps followed for the preparation of TY-loaded HNTs/PDA hybrid. (B) TEM images of pristine HNTs (i–iii), showing their characteristic tubular morphology and open-ended lumen, and the HNTs/PDA hybrid (iv–vi) obtained following the synthetic steps in A, depicting a thin layer that coats the nanotubes. (C) Elemental profile of Al (black) and C (blue) for (i) PDA-coated HNTs and (ii) HNTs measured by STEM-EDX. The presence of the analyzed elements is schematically illustrated at the bottom of (i). Insets depicting the analyzed clay nanotubes with the profile trace indicated in orange. For further details please refer to Fig. S3 in the ESI.†

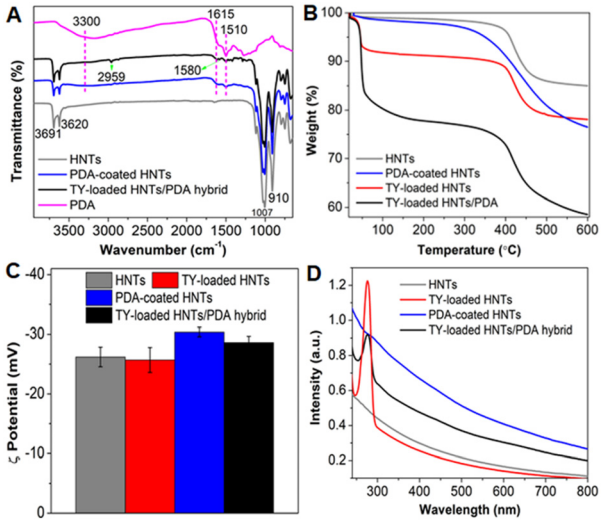

Fig. 2 Characterization of the TY-loaded HNTs/PDA hybrid. (A) ATR-FTIR spectra of pristine HNTs, PDA, PDA-coated HNTs, and TY-loaded HNTs/PDA hybrid. (B) TGA curves of pristine HNTs, PDA, TY-loaded HNTs, PDA-coated HNTs, and TY-loaded HNTs/PDA hybrid. (C) Zeta potential values and (D) UV-visible absorbance spectra of aqueous dispersions of pristine HNTs, TY-loaded HNTs, PDA-coated HNTs, and TY-loaded HNTs/PDA hybrid.

and electrostatic,[75,76] followed by polymerization. The presence of a PDA shell on various nanomaterials in the size range of 3–10 nm has been observed and reported before.[48,77–79]

The chemical composition of the hybrid following each of the synthetic steps, described in Fig. 1A, was studied using FTIR-ATR (Fig. 2A). The spectrum of HNTs depicts the signature bands at 910 cm^{-1}, 1007 cm^{-1}, 3620 cm^{-1}, and 3691 cm^{-1} corresponding to the O-H bending of inner hydroxyl groups, in-plane Si–O–Si symmetric stretching vibrations, inner AlO–H stretching vibrations, and O–H stretching of inner-surface hydroxyl groups, respectively (Fig. 2A black curve).[80] The spectrum of TY-loaded HNTs (Fig. S4A in the ESI,† red curve) depicts two new peaks at 2959 cm^{-1} and 1580 cm^{-1} corresponding to the CH and C=C stretching vibrations of TY, respectively,[62,81] which matches with the spectrum of pure TY (Fig. S4A in the ESI,† grey trace). After dopamine polymerization, the following additional peaks were observed: (i) a broad peak between 3140–3400 cm^{-1} corresponding to the -OH vibrations of catechol groups, (ii) less intense peaks at 1510 cm^{-1} and 1615 cm^{-1} ascribed to the shearing vibration of N-H in amide group and aromatic rings of PDA (see also Fig. S4B† for a detailed spectrum from 2000 to 600 cm^{-1}),[52] all of which match with the spectrum of pure PDA (Fig. 2A, magenta curve). In addition, the spectrum of TY-loaded HNTs/PDA hybrid (see also Fig. S4B† for a detailed spectrum from 2000 to 600 cm^{-1}) depicts all characteristic peaks that well correspond to HNTs, TY, and PDA, confirming the presence of all three components.

To complement these findings, we studied the weight change following each of the synthetic steps used for the fabrication of the TY-loaded HNTs/PDA hybrid by thermogravimetry and the results are presented in Fig. 2B. The pristine HNTs thermogram shows weight losses of 1% at a temperature range of 22 °C to 40 °C and of 13% between 300 °C and 530 °C, corresponding to the loss of moisture and dehydroxylation of structural Al-OH and Si-OH groups from HNTs, respectively.[82] After TY loading into the HNTs (TY-loaded HNTs), an additional weight loss of 6.6% (between 37 °C to 65 °C) is observed, confirming the successful loading of the EO (Fig. 2B and S5A† for pure TY). The thermogram of the TY-loaded HNTs/PDA hybrid (Fig. 2B, black curve) depicts a complex behavior, where weight losses at 37–65 °C (16.5%) and 300–530 °C (~13%) are ascribed to TY evaporation and HNT hydroxyls, respectively (Fig. S5B in the ESI† for the corresponding DTG curves for clarity). Since PDA decomposes over a wide temperature range[52,83] (see Fig. S5B ESI† for DTG curve of neat PDA), we have quantified the polymer content

in the hybrid according to its residue on a dry basis compared to that of pristine HNTs as depicted in Fig. S5C, ESI.† Accordingly, the PDA content is 8% and is in agreement with other studies,[42,75,84] confirming the successful formation of a PDA coating onto both pristine HNTs and TY-loaded HNTs.

The thermograms also reveal that the TY content in the hybrid is 2.7-fold higher than in the case of the TY-loaded HNTs (no PDA, see Table S1†). This can be attributed to the PDA layer which encapsulates the TY payload within the clay lumen and entraps the surface-physiosorbed TY molecules, retaining the EO during the washing step following the *in-situ* polymerization. Moreover, this can be also facilitated by non-covalent interactions (π–π and H-bonding) between the TY cargo and PDA, as was previously reported for several aromatic payloads such as the anticancer drug doxorubicin and the pesticide imidacloprid.[52,85] The DTG curves, presented in Fig. S3A-i and S3B (ESI†), reveal the profound effect of loading on the evaporation endpoint temperature of TY. The TY payload in the hybrid exhibits the highest value compared to TY-loaded HNTs (without PDA) and neat TY with values of 200, 65 and 55 °C, respectively. Thus, the substantial increase of the thermal stability of TY in the PDA-coated hybrid is mainly associated with former's encapsulation and entrapment by the polymer shell, while the adsorptive interactions at the clay surface[29,86] play a lesser role.

Zeta potential measurements of the HNTs aqueous dispersions (under neural pH) following each of the synthetic steps, detailed in Fig. 1A, were carried out to complement the surface characterization of the modified HNTs and the results are presented in Fig. 2C. Following dopamine polymerization, the zeta potential value of the HNTs (−26.2 ± 1 mV for pristine HNTs, attributed to the presence of negatively charged silica groups at the tubes' external surface)[87,88] is found to decrease to a value of −30.3 ± 0.7 mV. This may be ascribed to the deprotonated catechol–OH groups of PDA,[89,90] further supporting the formation of a PDA coating onto the nanotubes. A similar decrease was also obtained for the TY-loaded HNTs/PDA hybrid (−28.6 ± 0.1 mV), where it should be noted that TY loading resulted in only minor zeta potential change in comparison to the pristine HNTs, ascribed to the uncharged nature of TY.[91]

The optical properties for aqueous dispersions of the HNTs-based hybrids (1 mg mL^{-1}) were investigated by measuring their absorption spectra (Fig. 2D). In comparison to pristine HNTs, PDA-coated HNTs and TY-loaded HNTs/PDA hybrid show stronger absorbance in the UV-vis-NIR region, as contributed by the PDA shell.[78,92] For PDA-coated HNTs, the observed absorbance peak at 280 nm is assigned to the presence of a considerable fraction of dopamine in PDA.[79] The broad absorbance specifically towards the NIR region is attributed to the electronic properties of π–π* transition of polymeric backbone benzenoid ring,[93,94] and is favorable for photothermal therapy.[78] In addition, TY-loaded HNTs/PDA hybrid shows an intense absorbance peak at 278 nm, ascribed to the presence of TY.[62] A similar peak is also detected in the spectrum of the TY-loaded HNTs but without the pronounced PDA absorbance.

Thymol loading and release

Thymol was loaded into HNTs using the solvent evaporation method under vacuum and the resulting loaded HNTs were used for the subsequent dopamine polymerization followed by a washing step in DDW. Note that the control sample, TY-loaded HNTs without PDA, underwent a similar washing step using DDW following the loading process. Subsequently, thymol extraction was used to characterize the loading capacity of the modified HNTs. After careful composition tailoring, we found that for a ratio of 1.25 (HNTs) : 2.5(TY) : 1(PDA), the highest TY loading capacity of 14.7 ± 1.9% and encapsulation efficiency of 7.4 ± 1.0% is obtained. Notably, the latter TY content is ~2.5-fold higher in comparison to the corresponding TY-loaded HNTs (no PDA), where a loading capacity of only 5.6 ± 1.8% and encapsulation efficiency of 2.8 ± 0.9% is attained. These measured TY loading values are in good agreement with the calculated loading capacity based on the TGA data (see Fig. 2B and Table S1 in the ESI†). The

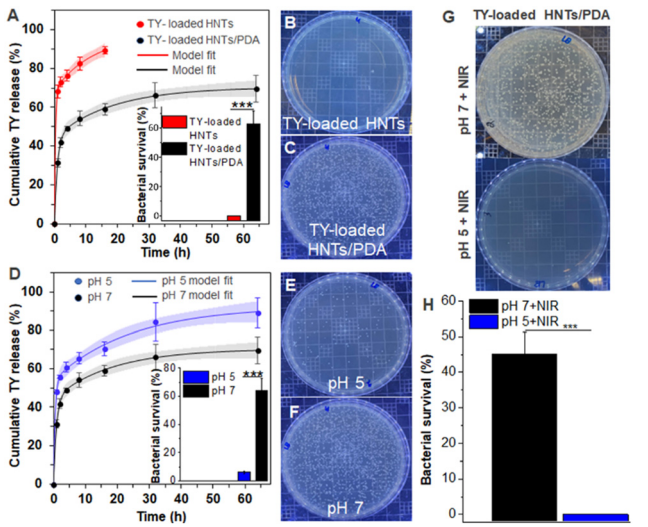

Fig. 3 (A) Thymol release profile from TY-loaded HNTs and TY-loaded HNTs/PDA hybrid in pH 7 buffer. (B and C) Representative images of Petri dishes seeded with *E. carotovora* exposed for 1 h at pH 7 to TY-loaded HNTs (B) and TY-loaded HNTs/PDA hybrid (C). Inset in A: showing the corresponding % bacterial survival. (D) pH-responsive release profile of TY from TY-loaded HNTs/PDA hybrid. (E and F) Representative images of Petri dishes seeded with *E. carotovora* exposed for 1 h to TY-loaded HNTs/PDA hybrid at pH 5 (E) and pH 7 (F) buffers. Inset in D: showing the corresponding % bacterial survival. (G) Representative images of Petri dishes seeded with *E. carotovora* exposed to TY-loaded HNTs/PDA hybrid at pH 5 and 7 following 15 min NIR irradiation at 808 nm with the corresponding % bacterial survival presented in (H). The significant difference between the groups was denoted by *** ($p < 0.001$), * (p = 0.01 to 0.05), and no asterisks or "ns" ($p \geq 0.05$); which signify highly significant, significant, and non-significant, respectively.

loaded TY molecules can be confined within the clay lumen and also physiosorbed onto the HNTs surface. During the *in situ* polymerization, PDA is suggested to encapsulate the lumen-confined TY molecules and sterically entrap those physiosorbed onto the clay surface,[85] reducing their loss during the consecutive washing step, and thus improving the loading capacity. Molecular interactions, including H-bonding and π–π interactions between the TY molecules and the catechol as well as the primary amine groups of PDA further facilitate the reattainment of these volatile molecules.[85,95]

The release of TY from the TY-loaded HNTs and the TY-loaded HNTs/PDA hybrid was investigated in a pH 7 buffer at 37 °C and the obtained profile is presented in Fig. 3A; where a double exponential model is applied with a very good fit to the experimental results ($R^2 > 0.97$ for TY-loaded HNTs/PDA and >0.9 for TY-loaded HNTs). The double exponential model describes a mass transfer regime comprising two different release sites simultaneously, one of them is more rapid than the other.[96,97] In our system, the fast and slow-release mechanisms are attributed to the TY adsorbed onto the clay surface and inside the HNTs lumen, respectively. For the PDA-coated hybrid (Fig. 3A), a 3-fold decrease in the rate constant of the fast-release component and a consecutive increase in its half-time (from 3 to 1 h) is obtained. Thus, the PDA shell polymerized on the nanotubes (see Fig. 1B-vi) hinders the burst release of the surface-adsorbed TY molecules. This assumption is further supported by the fact that the calculated parameters of the slow-release component, including the partition between fast and slow components were not significantly altered following the PDA coating. The slower release of TY from the PDA-coated hybrid can be also corroborated by its exerted antimicrobial properties as will be discussed in the next section.

PDA is well known for its stimuli-responsive properties, specifically pH and NIR irradiation,[98,99] and therefore its coating onto the loaded HNTs is expected to affect the TY release under different environmental conditions. First, the effect of pH on the TY release from TY-loaded HNTs/PDA hybrid was investigated and Fig. 3D depicts the accumulated release in pH 5 and 7. Under acidic conditions, the observed value of cumulative release was 20–30% higher in comparison to neutral conditions through most of the release study, as well as for the calculated release at infinite time. Nonetheless, no significant differences were observed in the release kinetics or partition between fast and slow components. A similar effect of acidic conditions on the plateau release value of other drugs and active compounds from PDA-coated hybrids has been reported before.[100,101] The acid-triggered release behavior of the TY-loaded HNTs/PDA hybrid further underscores its core–shell structure and is ascribed to conformational changes of the PDA shell due to the electrostatic repulsion of protonated amine groups possibly enabling higher equilibrium concentration of the released cargo.[89]

Antibacterial properties

The *in vitro* antibacterial activity against *E. carotovora* exerted by the TY-loaded HNTs and TY-loaded HNTs/PDA hybrids was investigated in a neutral buffer (pH 7) and the results (after 1 h incubation) are depicted in Fig. 3B and C, respectively (see also inset in Fig. 3A). The TY-loaded HNTs induced 100% bacterial inhibition, similar to the effect of a TY emulsion at an equivalent concentration (Fig. S6 in the ESI†). These results correspond to the burst release of TY from the nanotubes, where >70% of the TY was released within 1 h, as presented in Fig. 3A. The attained antibacterial effect of the TY-loaded HNTs/PDA hybrid after 1 h was moderate, compared to that of the TY-loaded HNTs, and consistent with the sustained release of TY from these coated nanotubes.

The effect of the PDA layer on the release of TY is further manifested when comparing the exerted antibacterial activity of the TY-loaded HNTs/PDA hybrid at different pH conditions. At pH 5, the hybrid's antibacterial activity was significantly enhanced, and 93% inhibition was obtained (Fig. 3E), demonstrating a 2.6-fold increase compared to neutral conditions, see inset in Fig. 3D. This finding is ascribed to accelerated TY release at a lower pH value as discussed in the previous section. It should be noted that pH alone has a negligible effect on the growth of *E. carotovora*, as shown in Fig. S6 in the ESI.†[102]

PDA's strong absorption in the NIR region and photothermal properties have motivated its exploitation as a coating material rendering surfaces with photo-responsive antimicrobial properties.[93,103,104] Thus, the effect of NIR irradiation on the exerted antibacterial properties of the developed hybrid was investigated. First, the photothermal properties of both the PDA-coated HNTs and the TY-loaded hybrid were characterized under irradiation with a NIR laser (15 min at 808 nm), and a significant temperature increase of >20 °C was detected, see Fig. S7 in the ESI.† Next, the antibacterial properties following irradiation were measured and the results are presented in Fig. 3G and H, where for the TY-loaded HNTs/PDA hybrid a complete bacterial inhibition at pH 5 is observed. At pH 7, the irradiation effect was weaker, and a 1.5-fold enhancement in bacterial inhibition was attained. Note that for the control PDA-coated HNTs (no TY), NIR irradiation induced only a 20% increase in bacterial inhibition, see Fig. S8 in the ESI.† Therefore, the superior photo-induced antibacterial efficacy of the TY-loaded hybrid can be ascribed to the combined effect of the photothermal activity of the PDA coating,[93,105,106] which was previously shown to damage bacterial cell-membrane and its constituents,[107,108] and the released TY payload. Thus, in the context of agriculture, the combination of solar NIR irradiation and naturally induced acidic conditions in plants may be harnessed to trigger the dual stimuli-responsive property of the loaded hybrids. Lower pH at bacterial infection sites in plants could be elicited by various factors including acidic cell-wall degrading enzymes secreted by

bacteria, such as polygalacturonase of *E. carotovora*[55,56,109,110] or pathogen-induced acidification of plant organelles,[57] as well as acidic signaling compounds including ethylene produced by plants in response to infection.[111]

Interactions of HNT-based carriers with tomato leaf surface

Uptake of HNTs and PDA-coated HNTs in leaves. The uptake of nanoparticles (NPs) by the plant roots and foliar could lead to their accumulation and entry into the food chain. Various physiochemical properties of NPs such as size, aspect ratio, and charge were found to affect their uptake and translocation in plants.[112,113] Yet, only few works have addressed the behavior of HNTs, where their potential to be adsorbed and accumulated in plants *via* their roots was demonstrated,[35,87] raising safety concerns.

Taking these observations into consideration, we investigated the potential uptake of HNTs *via* foliar routes for model tomato plants. Both pristine HNTs and PDA-coated HNTs were labeled with FITC, see ESI† for fluorescence spectra in Fig. S9, and imaged by confocal microscopy. Fig. 4A depicts the reconstructed 3D z-stacking images, taken from the leaf epidermis to mesophyll cells. The labeled HNTs and hybrid particles are observed only on the leaf surface (where the chloroplast autofluorescence is observed as magenta). Moreover, Pearson's coefficient analysis (P = 0) confirms no correlation between the fluorescence signal of the nanotubes and that of the chloroplasts, see Fig. S10 in the ESI† for additional information. The orthogonal views, presented in Fig. 4B, allow further localization of the particles in deeper x–z and y–z directions of the leaf, where again no overlapping of the FITC fluorescence and chloroplast autofluorescence is observed. The fluorescence from both labeled HNTs and PDA-coated HNTs is detected only from the epidermal cell layer (Fig. S11 in the ESI†) and no FITC fluorescence can be observed in the mesophyll cells (see Fig. 4A and S10 in the ESI†). Thus, these results indicate that the nanotubes are localized on and within the epidermis layer, without penetrating inside the leaf, suggesting their potential as a safe nanocarrier for the delivery of active payloads.

Phytotoxicity of HNTs and PDA-coated HNTs in tomato plants. Next, we investigated the phytotoxicity of HNTs and PDA-coated HNTs towards tomato plants, as only very few studies reported plant-NPs interactions in general and nanotubes in particular.[35,114] NPs can induce numerous adverse effects on plants, including cell membrane damage and chlorophyll synthesis disruption at the cellular level, as well as distinct physiological changes.[115] The integrity of the leaf cell membrane was characterized after foliar exposure to HNTs and PDA-coated HNTs for 5 days; whereby the treated leaves were stained with PI dye and imaged by a confocal microscope (see Fig. S12 in the ESI†). Note that PI is a membrane-impermeable dye and as such it only stains DNA and RNA within cells with compromised membranes. Fig. 4C summarizes the results of the confocal studies, in terms of

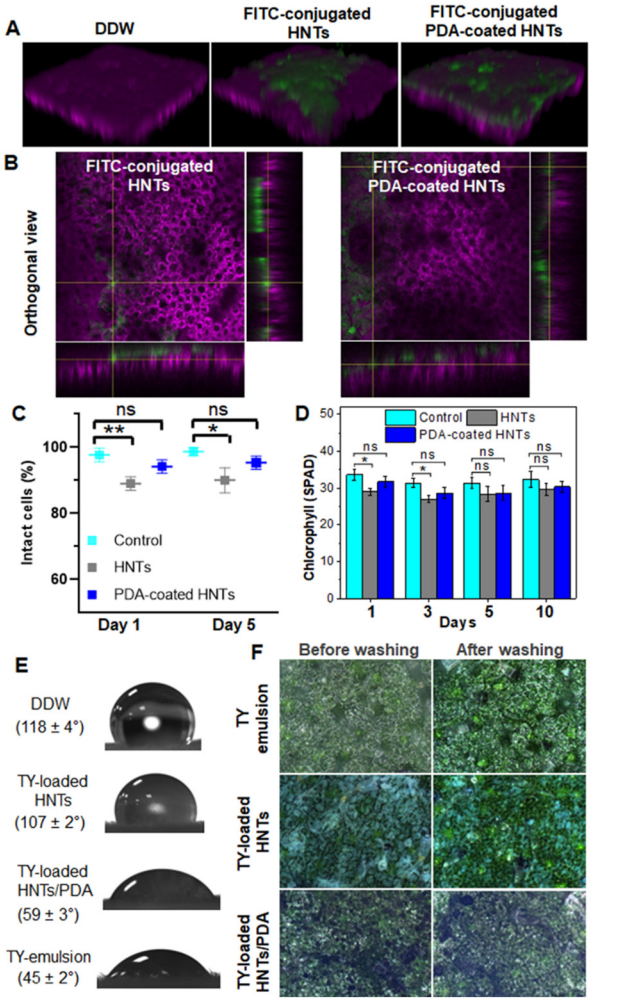

Fig. 4 Interactions of HNT-based carriers with tomato leaves. (A) 3D confocal images and (B) orthogonal views of leaves after 24 h incubation with FITC-conjugated HNTs and FITC-conjugated PDA-coated HNTs (scale bar = 30 μm). Green color indicates FITC fluorescence from nanotubes (Ex. λ = 488 nm) and magenta color indicates chloroplast autofluorescence (Ex. λ = 633 nm). Both orthogonal and 3D views of representative confocal z-stacks display no colocalization of nanocarriers with chloroplasts. (C) Quantitative analysis of intact plant cells reported as % of total cell number based on confocal images of leaves treated with DDW (control), HNTs, and PDA-coated HNTs. (D) The chlorophyll content of tomato leaves, measured after treatment with DDW (control), HNTs, and PDA-coated HNTs using a chlorophyll meter. (E) Images showing the contact angle of droplets of water, suspensions of TY-loaded HNTs, and TY-loaded HNTs/PDA hybrid, as well as TY emulsion on leaf surface. (F) Light microscopy images showing the adhesion ability of TY emulsion, TY-loaded HNTs, and TY-loaded HNTs/PDA hybrid on sprayed leaf surfaces before and after washing with DDW. The significant difference between the groups was denoted by * (p = 0.01 to 0.05) and no asterisks or "ns" ($p \geq 0.05$); which signify significant and non-significant, respectively.

the percentage of intact cells, after 1 and 5 days of exposure to the nanotubes. For both HNTs and PDA-coated HNTs >90% of cells displayed intact membrane even after 5 days of treatment, while the PDA-coated HNTs exhibit a marginally better compatibility with the tomato leaf cells in comparison

to pristine HNTs. This may be ascribed to the modified surface properties of the HNTs by the PDA coating.[116] Moreover, the effect of the clay nanotubes on the chlorophyll content in the leaf was characterized up to 10 days following treatment, and the results are summarized in Fig. 4D. PDA-coated HNTs are found to elicit no significant effect on the chlorophyll content. Conversely, for pristine HNTs, a small decrease in chlorophyll content was detected at days 1 and 3 exposure; yet this trend was not significant at day 10. Thus, these preliminary results imply that the presented PDA-coated clay nanocarrier is a viable option for foliar application in tomato plants, with no apparent phytotoxic effects.

Wetting and adhesion to leaves. Foliar retention of the nanocarriers, following their application, is critical for the efficient delivery of their bioactive cargo.[117] As such, leaf surface wettability is of utmost importance as it is the preceding step to the leaf adhesion of the respective droplets, as well as their spreading, and retention on the leaf.[118] The tomato leaf, used as a model in this work, presents a characteristic high water contact angle of 118 ± 4° which prevents its wetting (see Fig. 4E).[119] Accordingly, the wetting behavior of aqueous dispersions containing the loaded nanotubes was investigated and Fig. 4E presents images of the respective droplets on the leaf surface including the measured contact angle values. The high contact angle value of the TY-loaded HNTs dispersion (107 ± 2°), indicative of poor wetting, is significantly decreased to a value of 59 ± 3° when PDA coating is used. Thus, the hybrid formulation presents an improved leaf wettability, comparable to that of a TY-emulsion (where Tween-80 is used as a surfactant), see Fig. 4E.

A complementary light microscopy study (using an upright reflectance microscope) reveals the accumulation of the different HNTs-based carriers on the leaf cuticle following their application *via* spraying (Fig. 4F, left panel). Note that the deposition of the hybrid particles on the leaf surface can be easily observed by their distinct dark color in comparison to the corresponding whitish TY-loaded HNTs. Nanocarriers with high-aspect ratio, such as HNTs, are suggested as advantageous for foliar applications given their higher contact area in comparison to spherical particles.[117] The retention of the loaded carriers onto the plant leaves was qualitatively evaluated following their wash with water and the respective micrographs are depicted in Fig. 4F, right panel. The PDA-coated carriers exhibit greater retention on the leaf surface in comparison to TY-loaded HNTs, which can be ascribed to the enhanced wettability provided by the PDA as well as to the strong adhesion provided by the catechol side chains of PDA, which can strongly bind to various types of surfaces.[46,47,120] Moreover, the formation of different interactions (H-bonding, electrostatic, and covalent Schiff base) between the PDA hydroxyls and amines and functional groups on leaf surface (complex fatty acids, fatty alcohols, and fatty aldehydes) have been previously suggested.[65,120] Thus, these results demonstrate the superior foliar adhesion and retention of the hybrid carriers, which can potentially provide long-term efficacy.

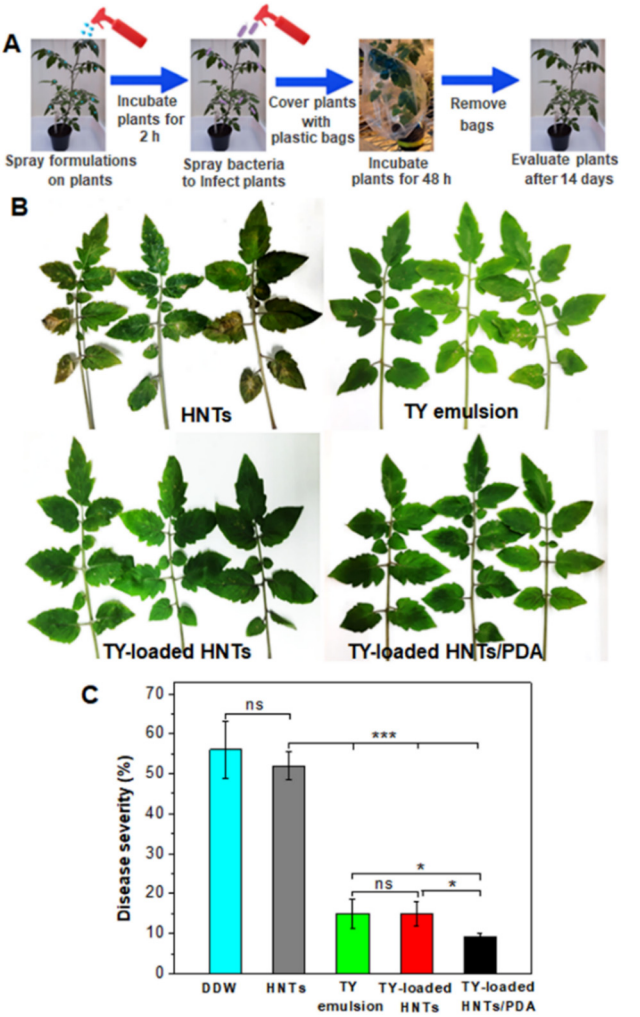

Fig. 5 *In planta* efficiency of different TY formulations against *E. carotovora*. (A) Schematic diagram showing the stepwise process for evaluating the antibacterial activity of different formulations against *E. carotovora* in tomato plants. (B) Images showing the incidence of bacterial lesions on plants treated with DDW (control), HNTs, TY emulsion, TY-loaded HNTs, and TY-loaded HNTs/PDA hybrid. (C) Plant bacterial disease severity (%) following treatment with DDW, HNTs dispersion, TY emulsion (used as a positive control), TY-loaded HNTs, and TY-loaded HNTs/PDA hybrid. The significant difference between the groups was denoted by *** ($p < 0.001$), * (p = 0.01 to 0.05), and no asterisks or "ns" ($p \geq 0.05$); which signify highly significant, significant, and non-significant, respectively.

Efficacy of TY-loaded HNTs/PDA hybrid against soft rot disease

The potential of the TY-loaded HNTs/PDA hybrid to suppress the soft rot disease of tomato plants was investigated and compared to that of TY-loaded HNTs and TY emulsion. The latter was used as a positive control at an optimized concentration of 0.4 mg mL^{-1}, corresponding to previously reported values which were demonstrated as effective in

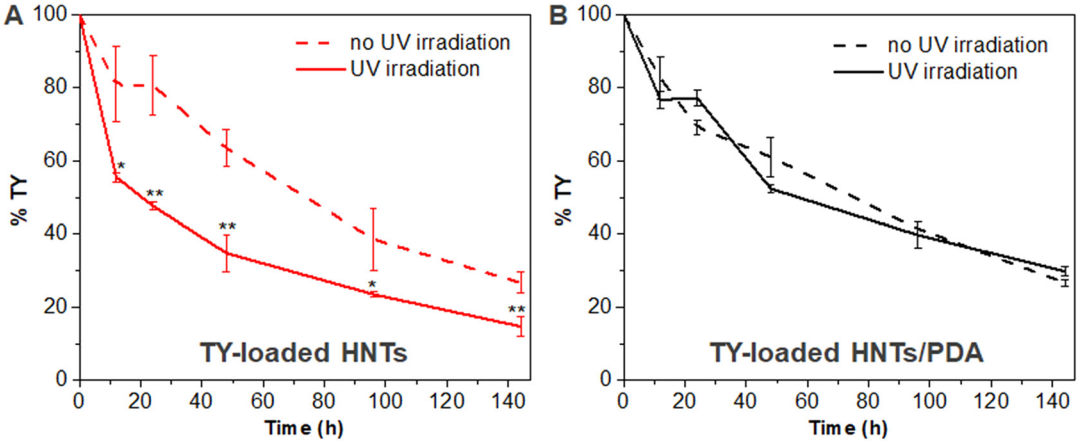

Fig. 6 Retention of TY in different HNTs-based carriers upon UV irradiation. Comparison of the residual TY content in (A) TY-loaded HNTs and (B) TY-loaded HNTs/PDA hybrid w/ and w/o UV irradiation at different time points. The significant difference between the groups was denoted by ** (p = 0.001 to 0.01), * (p = 0.01 to 0.05), and no asterisks ($p \geq 0.05$); which signify highly significant, significant, and non-significant, respectively.

reducing >50% bacterial infection on plants.[121,122] The concept of the study is presented in Fig. 5A, where tomato plants were first treated with the respective dispersion and then inoculated with *E. carotovora* bacterial suspensions. Plants treated with just DDW (see Fig. S13 in the ESI†) exhibit bacterial spots with coalescence on leaflets with a disease severity index (DSI) of >50%, demonstrating the ability of *E. carotovora* to severely infect the leaves.

Fig. 5B displays representative images of foliage treated with the respective formulations. All TY-containing treatments are shown to suppress to some extent the disease visual symptoms in comparison to plants treated with HNTs dispersion (or DDW). Quantitative analysis of the treatment's efficacy on disease severity (Fig. 5C), expressed in terms of % DSI, reveals that pristine HNTs have no significant antibacterial activity. In the case of TY-loaded HNTs (as well as TY emulsion used as a positive control), a significant reduction in DSI to ~15% is realized, where leaflets do not display any coalescence of bacterial spots but show sporadic necrotic symptoms (see Fig. 5B). Interestingly, analysis of leaves treated with TY-loaded HNTs/PDA confirms the superior efficacy of the developed nano-formulation in mitigating the soft rot disease in comparison to other treatments, which may be attributed to the controlled release behavior of the hybrid carrier. Furthermore, the hybrid could retain its disease control effect under drift conditions due to the good wettability and exceptional adhesion ability provided by the catechol moieties of the PDA even under wet conditions.[47,123] We note that the photothermal activity of the hybrid nanocarriers could potentially enhance even further their antibacterial activity of the released TY under sunlight, yet this was challenging to demonstrate in a greenhouse experiment.

TY Stability under UV irradiation

A wide range of volatile EOs, including TY, have been reported to be chemically unstable under various environmental conditions (*e.g.*, light, heat, air) resulting in deteriorated biological activity.[124] Several studies reported that encapsulation of EOs in different nanocarriers allows them to retain their exerted biological activity by reducing their volatility.[26,124–127] As the designed HNT-based carriers should function under varying UV conditions, we studied their chemical stability under UV irradiation and the results are depicted in Fig. 6. The TY-loaded HNTs/PDA hybrid (Fig. 6B) is found to exhibit superior retention of TY in comparison to the loaded HNTs (Fig. 6A) throughout the 144 h-long study. Notably, there are no significant differences in the extracted TY content w/ and w/o UV irradiation for the TY-loaded HNTs/PDA hybrid. However, in the case of the TY-loaded HNTs, UV irradiation is found to induce a profound and significant decrease in the residual TY content. After 48 h of UV exposure, the TY content decreased to a value of 34.8 ± 5.1% for the TY-loaded HNTs, and the residual TY content at the end of the experiment was lower than 15%, see Fig. 6A. In comparison, for the HNTs/PDA hybrid, TY content after 48 h was 52.4 ± 0.9% and 29.8 ± 1.3% at the end of the study (144 h), see Fig. 6B. This 1.5-fold difference in TY content between the carriers is attributed to the UV-shielding property of the PDA shell which covers the HNTs,[50] and minimizes TY loss, which is highly advantageous for foliar application of these carrier.

Conclusions

This study presents a stimuli-responsive core–shell agro-nanocarrier which is easily fabricated from natural compounds *via in situ* polymerization of dopamine on clay HNTs loaded with the antibacterial essential oil, thymol (TY). The resulting TY-loaded HNTs/PDA hybrid demonstrates superior efficiency in protecting tomato plants from soft rot disease, as demonstrated *in planta* by real-scenario greenhouse experiments. This superior crop protection

performance is ascribed to the advantageous attributes of the PDA-coated nanocarrier, as detailed below.

The 10 nm thick layer of PDA, polymerized on the clay nanotubes, is shown to significantly improve the loading capacity of TY and allows for its sustained and prolonged release in comparison to TY-loaded HNTs lacking the PDA compound. Moreover, the unique chemical composition of PDA allows for a dual-stimuli-triggered TY release under acidic conditions (characteristic of plant bacterial infection site) and *via* a photothermal effect upon exposure to NIR irradiation (which mimics the NIR irradiation in sunlight). This is corroborated by *in vitro* results demonstrating that both stimuli induce an intensification of the antibacterial effect exerted by the developed hybrid against *E. carotovora*, the bacterial pathogen responsible for the soft rot disease.

Regarding formulation stability, a rain simulation experiment reveals that the formulation is highly resistant to wash-out from the leaf surface. In addition, the PDA layer enhances TY's chemical stability under UV irradiation, potentially minimizing the loss of the active ingredient under sunlight. Both of these attributes can maintain the long-term bioactivity of the loaded compound by reducing its loss to the environment, thereby rendering the formulation more sustainable and cost-effective.

Furthermore, 3D confocal images demonstrate that the PDA-coated clay particles remain on the leaf's epidermis layer without being internalized through foliar uptake routes, obviating the formulation's phytotoxicity and potential entry into the food chain.

Our findings underscore the significant potential of the designed PDA-coated clay-based nanocarrier to enhance the effectiveness, stability, and safety of biocide application in plant pathogen control. In addition to antimicrobial agents, the presented system could be utilized in the future as a generic platform for the controlled release of a broader range of bioactive compounds, including plant growth regulators, protecting crops from diseases, promoting healthy plant growth, and improving overall yield.

Author contributions

S. S. conceived the idea of PDA coating; synthesized and characterized the properties of the nanocarriers; performed: loading and release experiments, stability study, *in vitro* antibacterial assay, plant-HNTs interactions experiments, and in-planta efficacy studies of the nano-formulations. He also wrote the first draft. O. P. S. carried out all the electron microscopy studies, analysed the release and thermogravimetry data, and participated in writing and revising the manuscript. H. A. H. assisted in performing the *in-vitro* antibacterial assay and synthesizing the nanocarriers. E. S. supervised the study, and was responsible for funding acquisition, as well as contributed to data analysis, writing and revising the manuscript. All authors have read and agreed to the final version of the manuscript.

Conflicts of interest

The authors declare no competing financial interest.

Acknowledgements

This work was supported by the Israel Innovation Authority in the framework of the SMART consortium. The authors thank Dr. Michal Leshem for editing the manuscript.

References

1 *SDG 2*, Zero hunger | Sustainable Development Goals | Food and Agriculture Organization of the United Nations, **https://www.fao.org/sustainable-development-goals/goals/goal-2/en/**, (accessed 4 February 2023).
2 *FAOSTAT*, **https://fenix.fao.org/faostat/internal/en/#home**, (accessed 4 February 2023).
3 C. Erika, S. Griebel, M. Naumann and E. Pawelzik, *Front. Plant Sci.*, 2020, **11**, 589692.
4 Y. Aysan, F. Sahin, R. Cetinkaya-Yildiz, M. Mirik and F. Yucel, *J. Plant Dis. Prot.*, 2005, **112**(1), 42–51.
5 A. Akbar, S. ud Din, M. Ahmad, G. daraz Khan and S. Alam, *J. Nat. Sci. Res.*, 2014, **4**(11), 99–102.
6 A. M. Alippi, E. Dal Bó, L. B. Ronco, P. E. Casanova and O. M. Aguilar, *Plant Dis.*, 1997, **81**, 230.
7 N. Pradnyarani, M. S. Kulkarni, K. C. Kirankumar, R. K. Mesta and C. K. Chethankumar, *Int. J. Chem. Stud.*, 2018, **6**(4), 75–78.
8 Y. Kolomiiets, I. Grygoryuk, L. Butsenko, V. Bohoslavets, Y. Blume and A. Yemets, *Open Agric. J.*, 2020, **14**, 290–298.
9 W. Aktar, D. Sengupta and A. Chowdhury, *Interdiscip. Toxicol.*, 2009, **2**, 1.
10 G. W. Sundin, L. F. Castiblanco, X. Yuan, Q. Zeng and C. H. Yang, *Mol. Plant Pathol.*, 2016, **17**, 1506.
11 F. H. M. Tang, M. Lenzen, A. McBratney and F. Maggi, *Nat. Geosci.*, 2021, **14**, 206–210.
12 R. Nair, S. H. Varghese, B. G. Nair, T. Maekawa, Y. Yoshida and D. S. Kumar, *Plant Sci.*, 2010, **179**, 154–163.
13 T. C. Hoang, E. C. Rogevich, G. M. Rand, P. R. Gardinali, R. A. Frakes and T. A. Bargar, *Environ. Pollut.*, 2008, **154**, 338–347.
14 S. Sharma, B. Singh, P. Bindra, P. Panneerselvam, N. Dwivedi, A. Senapati, A. Adholeya and V. Shanmugam, *ACS Appl. Mater. Interfaces*, 2021, **13**, 9143–9155.
15 X. Zhao, H. Cui, Y. Wang, C. Sun, B. Cui and Z. Zeng, *J. Agric. Food Chem.*, 2018, **66**, 6504–6512.
16 R. C. Fierascu, I. C. Fierascu, C. E. Dinu-Pirvu, I. Fierascu and A. Paunescu, *Z. Naturforsch., C: J. Biosci.*, 2020, **75**, 183–204.
17 C. Regnault-Roger, C. Vincent and J. T. Arnason, *Annu. Rev. Entomol.*, 2012, **57**, 405–424.
18 A. T. H. Mossa, *J. Environ. Sci. Technol.*, 2016, **9**, 354–378.
19 A. Escobar, M. Pérez, G. Romanelli and G. Blustein, *Arabian J. Chem.*, 2020, **13**, 9243–9269.
20 F. Tao, L. E. Hill, Y. Peng and C. L. Gomes, *LWT–Food Sci. Technol.*, 2014, **59**, 247–255.

21 A. Marchese, I. E. Orhan, M. Daglia, R. Barbieri, A. Di Lorenzo, S. F. Nabavi, O. Gortzi, M. Izadi and S. M. Nabavi, *Food Chem.*, 2016, **210**, 402–414.
22 *Federal Register :: Thymol; Exemption from the Requirement of a Tolerance*, **https://www.federalregister.gov/documents/2006/01/18/06-436/thymol-exemption-from-the-requirement-of-a-tolerance**, (accessed 4 February 2023).
23 *eCFR :: 21 CFR Part 172 – Food Additives Permitted for Direct Addition to Food for Human Consumption*, **https://www.ecfr.gov/current/title-21/chapter-I/subchapter-B/part-172**, (accessed 4 February 2023).
24 M. Coimbra, B. Isacchi, L. Van Bloois, J. S. Torano, A. Ket, X. Wu, F. Broere, J. M. Metselaar, C. J. F. Rijcken, G. Storm, R. Bilia and R. M. Schiffelers, *Int. J. Pharm.*, 2011, **416**, 433–442.
25 G. M. Glenn, A. P. Klamczynski, D. F. Woods, B. Chiou, W. J. Orts and S. H. Imam, *J. Agric. Food Chem.*, 2010, **58**, 4180–4184.
26 A. R. Bilia, C. Guccione, B. Isacchi, C. Righeschi, F. Firenzuoli and M. C. Bergonzi, *J. Evidence-Based Complementary Altern. Med.*, 2014, **2014**, 651593.
27 A. Giannakas, I. Tsagkalias, D. S. Achilias and A. Ladavos, *Appl. Clay Sci.*, 2017, **146**, 362–370.
28 M. A. Kinninmonth, C. M. Liauw, J. Verran, R. Taylor, V. Edwards-Jones, D. Shaw and M. Webb, *Appl. Clay Sci.*, 2013, **83–84**, 415–425.
29 M. Krepker, R. Shemesh, Y. Danin Poleg, Y. Kashi, A. Vaxman and E. Segal, *Food Control*, 2017, **76**, 117–126.
30 M. H. Lee, H. S. Seo and H. J. Park, *J. Food Sci.*, 2017, **82**, 922–932.
31 E. Joussein, *Dev. Clay Sci.*, 2016, **7**, 12–48.
32 F. W. Degrazia, V. C. B. Leitune, A. S. Takimi, F. M. Collares and S. Sauro, *Dent. Mater.*, 2016, **32**, 1133–1143.
33 O. Prinz Setter and E. Segal, *Nanoscale*, 2020, **12**, 23444–23460.
34 H. Wei, H. Wang, H. Chu and J. Li, *Int. J. Biol. Macromol.*, 2019, **133**, 1210–1218.
35 L. Chen, Z. Guo, B. Lao, C. Li, J. Zhu, R. Yu and M. Liu, *Environ. Sci.: Nano*, 2021, **8**, 3015–3027.
36 A. C. Santos, C. Ferreira, F. Veiga, A. J. Ribeiro, A. Panchal, Y. Lvov and A. Agarwal, *Adv. Colloid Interface Sci.*, 2018, **257**, 58–70.
37 M. R. Dzamukova, E. A. Naumenko, Y. M. Lvov and R. F. Fakhrullin, *Sci. Rep.*, 2015, **5**, 1–11.
38 G. Fakhrullina, E. Khakimova, F. Akhatova, G. Lazzara, F. Parisi and R. Fakhrullin, *ACS Appl. Mater. Interfaces*, 2019, **11**, 23050–23064.
39 M. Massaro, G. Cavallaro, C. G. Colletti, G. Lazzara, S. Milioto, R. Noto and S. Riela, *J. Mater. Chem. B*, 2018, **6**, 3415–3433.
40 Y. Liu, K. Ai and L. Lu, *Chem. Rev.*, 2014, **114**, 5057–5115.
41 C. J. Bettinger, J. P. Bruggeman, A. Misra, J. T. Borenstein and R. Langer, *Biomaterials*, 2009, **30**, 3050–3057.
42 M. L. Alfieri, M. Massaro, M. d'Ischia, G. D'Errico, N. Gallucci, M. Gruttadauria, M. Licciardi, L. F. Liotta, G. Nicotra, G. Sfuncia and S. Riela, *J. Colloid Interface Sci.*, 2022, **606**, 1779–1791.
43 S. Yuce, O. Demirel, B. Alkan Tas, P. Sungur and H. Unal, *ACS Appl. Nano Mater.*, 2021, **4**, 13432–13439.
44 C. E. Taş, S. O. Gundogdu and H. Ünal, *ACS Appl. Nano Mater.*, 2022, **5**, 5407–5415.
45 M. J. Harrington, A. Masic, N. Holten-Andersen, J. H. Waite and P. Fratzl, *Science*, 2010, **328**, 216–220.
46 Y. Tong, L. Shao, X. Li, J. Lu, H. Sun, S. Xiang, Z. Zhang, Y. Wu and X. Wu, *J. Agric. Food Chem.*, 2018, **66**, 2616–2622.
47 J. Liebscher, *Eur. J. Org. Chem.*, 2019, **2019**, 4976–4994.
48 X. Li, C. Xie, H. Xia and Z. Wang, *Langmuir*, 2018, **34**, 9974–9981.
49 W. Nong, W. Guan, Y. Yin, C. Lu, Q. Wang, Y. Luo, B. Zhang, Z. Xu, J. Wu and Y. Guan, *Chem. Eng. J.*, 2021, **420**, 129874.
50 W. B. Sheng, W. Li, G. X. Zhang, Y. Bin Tong, Z. Y. Liu and X. Jia, *New J. Chem.*, 2015, **39**, 2752–2757.
51 Q. Zheng, T. Lin, H. Wu, L. Guo, P. Ye, Y. Hao, Q. Guo, J. Jiang, F. Fu and G. Chen, *Int. J. Pharm.*, 2014, **463**, 22–26.
52 Y. Sun and E. W. Davis, *J. Mater. Chem. B*, 2019, **7**, 6828–6839.
53 Y. Liang, C. Fan, H. Dong, W. Zhang, G. Tang, J. Yang, N. Jiang and Y. Cao, *ACS Sustainable Chem. Eng.*, 2018, **6**, 10211–10220.
54 Y. Shan, C. Xu, H. Zhang, H. Chen, M. Bilal, S. Niu, L. Cao and Q. Huang, *Nanomater.*, 2020, **10**, 2000.
55 W. Pagel and R. Heitefuss, *Physiol. Mol. Plant Pathol.*, 1990, **37**, 9–25.
56 S. R. Herron, J. A. E. Benen, R. D. Scavetta, J. Visser and F. Jurnak, *Proc. Natl. Acad. Sci. U. S. A.*, 2000, **97**, 8762–8769.
57 C. Kesten, F. M. Gámez-Arjona, A. Menna, S. Scholl, S. Dora, A. I. Huerta, H.-Y. Huang, N. Tintor, T. Kinoshita, M. Rep, M. Krebs, K. Schumacher and C. Sánchez-Rodríguez, *EMBO J.*, 2019, **38**, e101822.
58 Y. Liu, H. Guan, J. Zhang, Y. Zhao, J. H. Yang and B. Zhang, *Int. J. Hydrogen Energy*, 2018, **43**, 2754–2762.
59 X. Yu, D. He, X. Zhang, H. Zhang, J. Song, D. Shi, Y. Fan, G. Luo and J. Deng, *ACS Appl. Mater. Interfaces*, 2019, **11**, 1766–1781.
60 A. P. Tiwari, D. P. Bhattarai, B. Maharjan, S. W. Ko, H. Y. Kim, C. H. Park and C. S. Kim, *Sci. Rep.*, 2019, **9**, 1–13.
61 L. Keawchaoon and R. Yoksan, *Colloids Surf., B*, 2011, **84**, 163–171.
62 Y. Zhang, Y. Zhang, Z. Zhu, X. Jiao, Y. Shang and Y. Wen, *J. Agric. Food Chem.*, 2019, **67**, 1736–1741.
63 V. Vergaro, E. Abdullayev, Y. M. Lvov, A. Zeitoun, R. Cingolani, R. Rinaldi and S. Leporatti, *Biomacromolecules*, 2010, **11**, 820–826.
64 E. Papierowska, S. Szporak-Wasilewska, J. Szewińska, J. Szatyłowicz, G. Debaene and M. Utratna, *Trees*, 2018, **32**, 1253–1266.
65 M. Zhao, P. Li, H. Zhou, L. Hao, H. Chen and X. Zhou, *Chem. Eng. J.*, 2022, **435**, 134861.
66 S. Sharma, S. Singh, A. K. Ganguli and V. Shanmugam, *Carbon*, 2017, **115**, 781–790.

67 I. Ocsoy, M. L. Paret, M. A. Ocsoy, S. Kunwar, T. Chen, M. You and W. Tan, *ACS Nano*, 2013, **7**, 8972–8980.
68 K. D. Le, J. Kim, N. H. Yu, B. Kim, C. W. Lee and J. C. Kim, *Front. Plant Sci.*, 2020, **11**, 775.
69 K. S. Chiang, H. I. Liu and C. H. Bock, *Ann. Appl. Biol.*, 2017, **171**, 139–154.
70 J. L. D. Oliveira, E. V. R. Campos, A. E. S. Pereira, T. Pasquoto, R. Lima, R. Grillo, D. J. De Andrade, F. A. Dos Santos and L. F. Fraceto, *J. Agric. Food Chem.*, 2018, **66**, 1330–1340.
71 N. F. Della Vecchia, R. Avolio, M. Alfè, M. E. Errico, A. Napolitano and M. D'Ischia, *Adv. Funct. Mater.*, 2013, **23**, 1331–1340.
72 C. Battistella, N. C. Mccallum, K. Gnanasekaran, X. Zhou, V. Caponetti, M. Montalti and N. C. Gianneschi, *ACS Cent. Sci.*, 2020, **6**, 1179–1188.
73 V. S. Raman, S. Rooj, A. Das, K. W. Stöckelhuber, F. Simon, G. B. Nando and G. Heinrich, *J. Macromol. Sci., Part A: Pure Appl.Chem.*, 2013, **50**, 1091–1106.
74 H. Kang, X. Liu, S. Zhang and J. Li, *RSC Adv.*, 2017, **7**, 24140–24148.
75 S. Ganguly, T. K. Das, S. Mondal and N. C. Das, *RSC Adv.*, 2016, **6**, 105350–105362.
76 H. Lee, N. F. Scherer and P. B. Messersmith, *Proc. Natl. Acad. Sci. U. S. A.*, 2006, **103**, 12999–13003.
77 A. Kumar, S. Kumar, W. K. Rhim, G. H. Kim and J. M. Nam, *J. Am. Chem. Soc.*, 2014, **136**, 16317–16325.
78 L. Sen Lin, Z. X. Cong, J. B. Cao, K. M. Ke, Q. L. Peng, J. Gao, H. H. Yang, G. Liu and X. Chen, *ACS Nano*, 2014, **8**, 3876–3883.
79 J. J. Feng, P. P. Zhang, A. J. Wang, Q. C. Liao, J. L. Xi and J. R. Chen, *New J. Chem.*, 2011, **36**, 148–154.
80 X. Zhao, C. Zhou, Y. Lvov and M. Liu, *Small*, 2019, **15**, 1900357.
81 A. C. Solano Valderrama, G. Cecilia and R. De, *Am. J. Anal. Chem.*, 2017, **08**, 726–741.
82 S. Hamedi and M. Koosha, *Appl. Clay Sci.*, 2020, **197**, 105770.
83 H. Luo, C. Gu, W. Zheng, F. Dai, X. Wang and Z. Zheng, *RSC Adv.*, 2015, **5**, 13470–13477.
84 C. Chao, J. Liu, J. Wang, Y. Zhang, B. Zhang, Y. Zhang, X. Xiang and R. Chen, *ACS Appl. Mater. Interfaces*, 2013, **5**, 10559–10564.
85 X. Xu, B. Bai, H. Wang and Y. Suo, *ACS Appl. Mater. Interfaces*, 2017, **9**, 6424–6432.
86 R. Shemesh, M. Krepker, M. Natan, Y. Danin-Poleg, E. Banin, Y. Kashi, N. Nitzan, A. Vaxman and E. Segal, *RSC Adv.*, 2015, **5**, 87108–87117.
87 C. Wang, Z. He, Y. Liu, C. Zhou, J. Jiao, P. Li, D. Sun, L. Lin and Z. Yang, *Appl. Clay Sci.*, 2020, **198**, 105802.
88 O. Prinz Setter, A. Movsowitz, S. Goldberg and E. Segal, *ACS Appl. Bio Mater.*, 2021, **4**, 4094–4104.
89 L. Zha, J. Qian, B. Wang, H. Liu, C. Zhang, Q. Dong, W. Chen and L. Hong, *Int. J. Pharm.*, 2020, **587**, 119665.
90 M. Wu, C. Zhong, Q. Zhang, L. Wang, L. Wang, Y. Liu, X. Zhang and X. Zhao, *J. Nanobiotechnol.*, 2021, **19**, 1–17.
91 National Center for Biotechnology Information, PubChem Compound Summary for CID 6989, Thymol, **https://pubchem.ncbi.nlm.nih.gov/compound/Thymol**, Accessed Jan. 15, 2024.
92 J. H. Lin, C. J. Yu, Y. C. Yang and W. L. Tseng, *Phys. Chem. Chem. Phys.*, 2015, **17**, 15124–15130.
93 W. Lei, K. Ren, T. Chen, X. Chen, B. Li, H. Chang, J. Ji, W. X. Lei, K. Ren, T. T. Chen, X. C. Chen, B. C. Li, H. Chang and J. Ji, *Adv. Mater. Interfaces*, 2016, **3**, 1600767.
94 S. H. Kim, E. B. Kang, C. J. Jeong, S. M. Sharker, I. In and S. Y. Park, *ACS Appl. Mater. Interfaces*, 2015, **7**, 15600–15606.
95 X. Wang, J. Zhang, Y. Wang, C. Wang, J. Xiao, Q. Zhang and Y. Cheng, *Biomaterials*, 2016, **81**, 114–124.
96 M. Massaro, A. Borrego-Sánchez, R. Sánchez-Espejo, C. Viseras Iborra, G. Cavallaro, F. García-Villén, S. Guernelli, G. Lazzara, D. Miele, C. I. Sainz-Díaz, G. Sandri and S. Riela, *Appl. Clay Sci.*, 2021, **215**, 106310.
97 G. Lazzara, S. Riela and R. F. Fakhrullin, *Ther. Delivery*, 2017, **8**, 633–646.
98 H. Ma, S. Li, H. Zhang, Y. Wei and L. Jiang, *Colloids Surf., A*, 2019, **561**, 332–340.
99 H. Zhang, X. Wang, P. Wang, R. Liu, X. Hou, W. Cao, R. Zhong, X. Liu and Y. Zhang, *RSC Adv.*, 2018, **8**, 37433–37440.
100 Z. Zhu and M. Su, *Nanomater.*, 2017, **7**(7), 160.
101 C. Wang, J. Bai, Y. Liu, X. Jia and X. Jiang, *ACS Biomater. Sci. Eng.*, 2016, **2**, 2011–2017.
102 P. Laurent, L. Buchon, J. F. Burini and N. Orange, *Biotechnol. Lett.*, 2001, **23**, 753–756.
103 T. S. Sileika, H. Do Kim, P. Maniak and P. B. Messersmith, *ACS Appl. Mater. Interfaces*, 2011, **3**, 4602–4610.
104 C. Y. Liu and C. J. Huang, *Langmuir*, 2016, **32**, 5019–5028.
105 D. Hu, L. Zou, B. Li, M. Hu, W. Ye and J. Ji, *ACS Biomater. Sci. Eng.*, 2019, 5169–5179.
106 N. M. O. Andoy, K. Jeon, C. T. Kreis and R. M. A. Sullan, *Adv. Funct. Mater.*, 2020, **30**, 2004503.
107 P. Chandra Ray, S. Afrin Khan, A. Kumar Singh, D. Senapati and Z. Fan, *Chem. Soc. Rev.*, 2012, **41**, 3193–3209.
108 E. Ju, Z. Li, M. Li, K. Dong, J. Ren and X. Qu, *Chem. Commun.*, 2013, **49**, 9048–9050.
109 S. P. Lei, H. C. Lin, L. Heffernan and G. Wilcox, *J. Bacteriol.*, 1985, **164**, 831–835.
110 G. N. Agrios, *Plant Pathol.*, 2005, 124–174.
111 I. P. De León, J. P. Oliver, A. Castro, C. Gaggero, M. Bentancor and S. Vidal, *BMC Plant Biol.*, 2007, **7**, 1–11.
112 Y. Su, V. Ashworth, C. Kim, A. S. Adeleye, P. Rolshausen, C. Roper, J. White and D. Jassby, *Environ. Sci.: Nano*, 2019, **6**, 2311.
113 S. Sharma, B. K. Sahu, L. Cao, P. Bindra, K. Kaur, M. Chandel, N. Koratkar, Q. Huang and V. Shanmugam, *Prog. Mater. Sci.*, 2021, **121**, 100812.
114 E. González-Grandío, G. S. Demirer, C. T. Jackson, D. Yang, S. Ebert, K. Molawi, H. Keller and M. P. Landry, *J. Nanobiotechnol.*, 2021, **19**, 1–15.
115 J. Yanga, W. Cao and Y. Rui, *J. Plant Interact.*, 2017, **12**, 158–169.
116 S. Hong, K. Y. Kim, H. J. Wook, S. Y. Park, K. D. Lee, D. Y. Lee and H. Lee, *Nanomedicine*, 2011, **6**, 793–801.

117 R. Grillo, B. D. Mattos, D. R. Antunes, M. M. L. Forini, F. A. Monikh and O. J. Rojas, *Nano Today*, 2021, **37**, 101078.
118 J. J. Nairn and W. A. Forster, *Pest Manage. Sci.*, 2024, **80**(2), 212–219.
119 G. Yokoyama, D. Yasutake, T. Tanizaki and M. Kitano, *Photosynthetica*, 2019, **57**(3), 740–747.
120 T. Wu, X. Fang, Y. Yang, W. Meng, P. Yao, Q. Liu, B. Zhang, F. Liu, A. Zou and J. Cheng, *J. Agric. Food Chem.*, 2020, **68**, 12549–12557.
121 S. Kumari, R. C. Choudhary, R. V. Kumaraswamy, D. Bhagat, A. Pal, R. Raliya, P. Biswas and V. Saharan, *Plant Physiol. Biochem.*, 2019, **145**, 64–74.
122 S. Kumari, R. V. Kumaraswamy, R. C. Choudhary, S. S. Sharma, A. Pal, R. Raliya, P. Biswas and V. Saharan, *Sci. Rep.*, 2018, **8**, 1–12.
123 M. L. Alfieri, L. Panzella, S. L. Oscurato, M. Salvatore, R. Avolio, M. E. Errico, P. Maddalena, A. Napolitano and M. d'Ischia, *Biomimetics*, 2018, **3**, 26.
124 H. M. C. Marques, *Flavour Fragrance J.*, 2010, **25**, 313–326.
125 A. Celebioglu, Z. I. Yildiz and T. Uyar, *Food Res. Int.*, 2018, **106**, 280–290.
126 M. Christofoli, E. C. C. Costa, K. U. Bicalho, V. de Cássia Domingues, M. F. Peixoto, C. C. F. Alves, W. L. Araújo and C. de Melo Cazal, *Ind. Crops Prod.*, 2015, **70**, 301–308.
127 N. Massad-Ivanir, A. Sand, N. Nitzan, E. Valderama, M. Kurczewski, H. Remde, A. Wegenberger, K. Shlosman, R. Shemesh, A. Störmer and E. Segal, *Food Packag. Shelf Life*, 2023, **37**, 101079.